POLITECNICO DI TORINO
Repository ISTITUZIONALE

Application of UV absorbance and fluorescence indicators to assess the formation of biodegradable
dissolved organic carbon and bromate during ozonation

(Article begins on next page)

08 November 2022

Application of UV absorbance and fluorescence indicators to assess the formation of biodegradable dissolved organic carbon and bromate during ozonation

Wen-Tao Li [a, b, *], Meng-Jie Cao [b], Tessora Young [b], Barbara Ruffino [c], Michael Dodd [b], Ai-Min Li [a,*], Gregory Korshin [b]

[a] State Key Laboratory of Pollution Control and Resources Reuse, School of the Environment, Nanjing University, Nanjing, 210023, China

[b] Department of Civil & Environmental Engineering, University of Washington, Box 352700, Seattle, WA 98195-2700, United States

[c] Department of Environment, Land and Infrastructure Engineering, Politecnico di Torino, Corso Duca degli Abruzzi, 24 10129 Torino, Italy

CORRESPONDING AUTHOR FOOTNOTE：

Prof. Ai-Min Li
Email: liaimin@nju.edu.cn

Wen-Tao Li
Email: liwentaoepa@hotmail.com; liwentaonju@163.com

1 **Abstract:**

2 This study examined the significance of changes of UV absorbance and

3 fluorescence of dissolved organic matter (DOM) as surrogate indicators for assessing

4 the formation of bromate and biodegradable dissolved organic carbon (BDOC) during

5 the ozonation of surface water and wastewater effluent. Spectroscopic monitoring was

6 carried out using benchtop UV/Vis and fluorescence spectrophotometers and a newly

7 developed miniature LED UV/fluorescence sensor capable of rapidly measuring

8 UVA280 and protein-like and humic-like fluorescence. With the increase of O_3/DOC

9 mass ratio, the plots of BDOC formation were characterized of initial lag, transition

10 slope and final plateau. With the decrease of UV absorbance and fluorescence, BDOC

11 concentrations initially increased slowly and then rose more noticeably. Inflection

12 points in plots of BDOC versus changes of spectroscopic indicators were close to 35-

13 45% loss of UVA254 or UVA280 and 75-85% loss of humic-like fluorescence.

14 According to the data from size exclusion chromatography (SEC) with organic carbon

15 detection and 2D synchronous correlation analyses, DOM fractions assigned to

16 operationally defined large biopolymers (apparent molecular weight, AMW>20 kDa)

17 and medium AMW humic substances (AMW 5.5-20 kDa) were transformed into

18 medium-size building blocks (AMW 3-5.5 kDa) and other smaller AMW species

19 (AMW<3 kDa) associated with BDOC at increasing O_3/DOC ratios. Appreciable

20 bromate formation was observed only after the values of UVA254, UVA280 and

21 humic-like fluorescence in O_3-treated samples were decreased by 45-55%, 50-60% and

22 86-92% relative to their respective initial levels. No significant differences in plots of

2

23 bromate concentrations versus decreases of humic-like fluorescence were observed for

24 surface water and wastewater effluent samples. This was in contrast with the plots of

25 bromate concentration versus UVA254 and UVA280 which exhibited sensitivity to

26 varying initial bromide concentrations in the investigated water matrixes. These results

27 suggest that measurements of humic-like fluorescence can provide a useful supplement

28 to UVA indices for characterization of ozonation processes.

29 **Keywords**: ozonation; biodegradable dissolved organic carbon; bromate; spectroscopic

30 indicator; humic substances; online fluorescence sensor

1. Introduction

32   Ozonation has been widely used in drinking water and wastewater treatment for

33 disinfection and oxidation purposes (Reungoat et al. 2012, von Gunten 2003a, b,

34 Zimmermann et al. 2011). Extensive studies have shown that ozonation results in

35 significant elimination of adverse biological effects of many organic micropollutants

36 (e.g., endocrine disrupting chemicals, antibiotics, and pharmaceuticals) as well as

37 removal of color, odor and taste (Dodd et al. 2009, Hollender et al. 2009, Huber et al.

38 2005, Lee et al. 2012, Liu et al. 2012a, Nakada et al. 2007, Peter and von Gunten 2007).

39   Ozone exposures required for disinfection and oxidation may result in the

40 formation of undesirable organic and inorganic byproducts, including various

41 disinfection byproducts (DBPs) and biodegradable dissolved organic carbon (BDOC)

42 (von Gunten 2003b, Wert et al. 2007). Ozonation has been shown to convert relatively

43 refractory components of dissolved organic matter (DOM) into BDOC (e.g., aldehydes,

44 carboxylic acids, ketones and etc.) without a significant decrease in overall dissolved

45 organic carbon (DOC) concentration (Liu et al. 2015, Nishijima et al. 2003, Wert et al.

46 2007). The ozonation-derived BDOC in turn largely defines the biological stability of

47 ozonated water, as it can contribute to increases in bacterial regrowth in drinking water

48 distribution systems or wastewater effluent receiving waters (Escobar and Randall

49 2001). As a result, ozonation is usually combined with a subsequent process of

50 biological filtration to consume BDOC before the treated water is conveyed into a

51 distribution system or a receiving water body. In this context, characterization of

52 changes of molecular weights (MW) of DOM and evaluation of BDOC formation may

53   provide a better understanding of integrated O_3 biofiltration processes for DOC removal.

54   In addition, ozonation of bromide-containing water or wastewater leads to the

55   formation of bromate (von Gunten and Oliveras 1998). Bromate is classified as a

56   probable or likely human carcinogen, and many countries have established the

57   maximum allowable level of bromate in drinking water at 10 µg/L (Butler et al. 2005).

58   Unlike many organic DBPs, bromate is relatively stable and is difficult to remove using

59   conventional treatment technologies (Butler et al. 2005, Nie et al. 2014). Although

60   ecological impacts of bromate formation during wastewater ozonation are uncertain,

61   the potential public health implications of bromate formation in potable water reuse

62   scenarios utilizing ozonation could be significant. Hence it is of substantial interest to

63   develop tools for better predicting and controlling bromate concentrations formed

64   during both drinking water and wastewater ozonation.

65   The formation of BDOC and bromate, as well as the elimination of micropollutants,

66   are directly related to the ozone exposure ($\int_0^t [O_3]dt$); that is, the time-dependent ozone

67   concentration integrated over exposure time. An optimization of the ozone exposure is

68   necessary to maximize the effect of oxidation and minimize the formation of undesired

69   DBPs, especially BrO_3^-. However, for wastewater effluents, it is difficult to measure a

70   dissolved O_3 residual during the initial O_3 demand stage (Gerrity et al. 2012, Wert et al.

71   2009). Additionally, direct analyses of BDOC and bromate are time-consuming and

72   expensive. Therefore, the development of surrogate parameters for frequent online

73   monitoring to enable more automated controls of ozone dosage is warranted. For

74   example, the California Department of Public Health recently published a revised set

75   of draft regulations for groundwater replenishment, which requires full advanced

76   treatment facilities to identify at least one surrogate parameter that can be monitored

77   continuously (Chon et al. 2015, Gerrity et al. 2012).

78   A number of studies have examined the performance of spectroscopic indicators,

79   such as color, differential UV absorbance (UVA) and/or total fluorescence, and shown

80   that such indicators were correlated with the removal efficiencies of organic

81   micropollutants during ozonation (Gerrity et al. 2012, Li et al. 2016b, Liu et al. 2012b,

82   Nanaboina and Korshin 2010, Wert et al. 2009). Recently, Chon et al. (2015) applied

83   the concept of electron donating capacity of DOM combined with UVA254

84   measurements to evaluate the degradation of micropollutants and the formation of

85   bromate. Other studies have assessed the use of UVA254 and related indices to quantify

86   the formation of individual ozonation byproducts associated with BDOC (Liu et al.

87   2012a).

88   Measurements of UV absorbance at 280 nm by means of UV light emitting diodes

89   (LEDs) provide an attractive, energy-efficient alternative to conventional UVA254

90   monitoring (Bridgeman et al. 2015, Tedetti et al. 2013). UVA280 has previously been

91   found to correlate well with DOM molecular weight and aromaticity and exhibit lower

92   spectral overlap than UVA254 with inorganic species such as NO_3^- and NO_2^- that may

93   interfere with measurements in many waters (Chin et al. 1994). In addition,

94   measurements of DOM fluorescence at selected excitation and emission wavelengths

95   provide a useful complement to UVA280 since fluorescence detection can also be

96   implemented using LEDs and can enable more selective monitoring of chemically

97 reactive protein-like and humic-like DOM components (Fimmen et al. 2007, Henderson

98 et al. 2009). We recently demonstrated the use of a miniaturized LED UV/fluorescence

99 sensor – capable of online measurement of UVA280, as well as protein-like and humic-

100 like fluorescence – to predict DBP formation during chlorination (Li et al. 2016a).

101   The present study employs a sensor of this type to determine whether UVA280 and

102 fluorescence indices may be used to develop correlations with BDOC and bromate

103 formed during the ozonation of surface water and wastewater. To this end, degradation

104 of DOM chromophores and fluorophores, MW changes, and formation of BDOC and

105 bromate were examined during ozonation of a set of surface water and wastewater

106 matrixes with varying initial bromide concentrations.

107 **2. Material and methods**

108 **2.1. Water matrixes and reagents**

109   Three water matrixes were used in the experiments described below. Secondary

110 municipal wastewater effluent samples were taken from the West Point Treatment Plant

111 in King County, WA (WWTP-I on Dec 14th, 2015 and WWTP-II on Feb 28th, 2016).

112 This plant uses high-rate oxygen activated sludge technology without denitrification.

113 The surface water was sampled from Lake Pleasant, which is a brown water eutrophic

114 lake in Bothell, WA. Basic water characteristics of these waters are shown in **Table 1**.

115 All the water samples were immediately filtered through a 0.45 μm membrane upon

116 collection and stored at 4 °C before use.

117   The following chemicals were used in this study: sodium bromide (Sigma-

118   Aldrich, >99%), sodium bromate (Sigma-Aldrich, >99%), polyethylene glycol

119   standards (Alfa Aesar), methylamine solution (Sigma-Aldrich, 40 wt. % in H_2O), and

120   potassium indigotrisulfonate (Sigma-Aldrich).

2.2. Ozonation batch experiments

122   Five semi-batch ozonation experiments were performed at room temperature (25

123   ± 2 °C) with the three water matrixes mentioned above to explore the formation of

124   BDOC and bromate and evolution of spectroscopic indices during exposure to ozone.

125   For the WWTP-I water matrix (DOC 5.82 mg/L), three semi-batch experiments were

126   undertaken with spiked bromide concentrations of 50 μg/L (WWTP-A, 322.9 μg/L total

127   Br^-), 100 μg/L (WWTP-B, 373.8 μg/L total Br^-) and 200 μg/L Br^- (WWTP-C, 491.6

128   μg/L total Br^-) respectively, to explore effects of initial Br^- concentration. For the

129   WWTP-II water matrix (DOC 6.93 mg/L), one ozonation semi-batch experiment was

130   performed using a 100 μg/L Br^- spike (WWTP-D, 301.5 μg/L total Br^-) as a comparison

131   with the WWTP-I experiments. Because Lake Pleasant water had a high DOC

132   concentration (14.87 mg/L), the water was diluted 2.5 times with Milli-Q water and

133   spiked with 100 μg/L Br^- (LP, 5.98 mg/L DOC and 116.1 μg/L total Br^-).

134   Ozone was generated by an oxygen-fed ozonator (IN USA AC-2025; Norwood,

135   MA, USA). The feed gas stream containing ozone was bubbled through 200 mL WWTP

136   effluent or 250 mL LP water samples contained in a 500 mL borosilicate glass gas-

137   washing bottle using a sintered glass gas diffuser at a flow rate of ~550 ml/min. In each

138   batch experiment, the ozone doses were varied as a function of ozonation times which

139   were 0, 2, 5, 10, 15, 20, 25*, 30, 40, 50*, 60, 100, 180 and 300** s (* specific for LP

140   series and ** specific for WWTP series). The residual O_3 concentrations in ozonated

141   samples were immediately measured according to the standard indigo method (Bader

142   and Hoigné 1981), where 1 mL of ozonated sample was immediately spiked into glass

143   vials containing 9 mL indigo solution, and then analyzed for residual absorbance at 600

144   nm by UV-Vis spectroscopy. The remainder of the ozonated sample volumes was

145   transferred into 250 mL glass bottles with caps. UVA and fluorescence indicators were

146   measured at least 2 hours after ozonation, allowing the residual ozone to naturally decay

147   without adding any quenching agent. Then the samples were stored at 4 ºC before other

148   analyses, which were done within 5 days for each batch.

149   Compared with directly spiking aliquots of ozone stock (Chon et al. 2015, Gerrity

150   et al. 2012), the semi-batch ozonation experiment has no dilution effect on the samples,

151   which facilitates the measurement of BDOC. However, the determination of ozone dose

152   becomes another important issue, as the rate of ozone mass transferred into water phase

153   may change as a function of time. As shown in **Figure S1,** the transferred/absorbed

154   ozone concentrations as a function of time were calculated based on measurements of

155   the differential O_3 concentrations between the feed gas and off-gas streams, where the

156   gaseous O_3 concentrations were measured by the modified indigo method (Chiou et al.

157   1995).

158   **2.3.   Batch biodegradation experiments**

159   BDOC measurements were performed by quantifying the gross amount of DOC

160   degraded by an inoculum of suspended activated sludge over a predetermined period of

161   time (Escobar and Randall 2001). In this study, a requisite amount of activated sludge

162   from a WWTP was initially acclimated with glucose for 3 days. The acclimated

163   activated sludge was washed by centrifugation and resuspended in deionized water 5

164   times prior to harvesting for BDOC measurements. Then 50 mL centrifuge tubes were

165   filled with 40 ml water samples and spiked with 1 mL of the harvested activated sludge.

166   The BDOC tests were conducted in duplicate and compared with results obtained using

167   Milli-Q water as a blank control. A 200 mg/L dry biomass concentration was used in

168   the tests. This dose was determined by weighing the biomass collected from ten test

169   tubes after BDOC experiments; the biomass was dried at 105 °C before weighing. The

170   inoculated centrifuge tubes were placed in an incubated shaker at 90 rpm and 25 °C for

171   a period of 4 hours, following which the samples were centrifuged and the supernatants

172   filtered through a 0.45μm PTFE filter for subsequent DOC and molecular weight

173   analysis. The measured BDOC reflects the rapidly biodegradable fraction of BDOC

174   that can be effectively removed by biofiltration; this fraction is thus referred to as

175    $BDOC_{rapid}$ henceforth (Black and Berube 2014).

176   **2.4. UV absorbance and fluorescence analysis**

177   A HORIBA Aqualog spectrometer was used to simultaneously measure

178   fluorescence EEM (Ex 220-450 nm / Em 245-825 nm) and UV absorbance spectra

179   (220-450 nm). The samples' EEMs were automatically corrected for Raman scattering

180   by subtracting the EEM of the water blank from the EEM of any surface water or

181   wastewater sample. Inner filter effects were corrected using the instrument's software

182   that utilized applicable absorbance data.

183   The prototype LED UV/fluorescence sensor described in more detail in (Li et al.

184   2016a) uses a UV LED (280 ± 5 nm) as a light source and a photodiode to measure the

185   intensity of light passing the cuvette. For fluorescence detection, the sensor uses blue

186   light sensitive photodiodes combined with bandpass filters (330-355 nm and 415-490

187   nm) positioned at 90° relative to the excitation beam to detect the protein-like and

188   humic-like fluorescence, respectively. Inner filter effects in fluorescence signals

189   detected by the sensor were corrected using the UVA280 values.

190   **2.5.   Molecular weight analysis**

191   Analyses of DOC molecular weight distributions were performed by means of size

192   exclusion chromatography with online carbon detection (SEC-OCD). These

193   measurements utilized a DIONEX Ultimate3000 high-pressure liquid chromatography

194   (HPLC) system coupled with an online organic carbon detector (Turbo Sievers 900

195   Portable TOC Analyzer, GE). A TOSOH Bioscience Toyopearl HW-50S size exclusion

196   column was installed to separate DOM components with varying apparent MWs. The

197   injection volume was 100 μL, and the column was eluted with 1 mL/min phosphate

198   buffer (1.5 g/L Na_2HPO_4 * 2 H_2O + 2.5 g/L KH_2PO_4). Polyethylene glycol standards

199   (PEG 20 kDa, 10 kDa, 6 kDa, 4 kDa, 1.5 kDa, 600 Da and 200 Da) from Alfa Aesar

200   were used as apparent molecular weight (AMW) references. The SEC-OCD

201   chromatograms for samples from each ozonation experiment were also processed with

202   Shige software developed by Noda and Ozaki (2005) for 2D correlation analysis – the

203 goal of which was to ascertain potentially small variations of various spectra resulting

204 from external perturbations, e.g., DOM ozonation in this study (supporting information

205 **Figure S4**).

206 **2.6. Bromide and bromate Analysis**

207   Bromide concentrations were determined by means of IC-ICP-MS, using a

208 PerkinElmer Series 200 HPLC coupled with a PerkinElmer SCIEX ELAN DRC-e

209 ICP/MS Spectrometer. These analyses were done in accord with prior investigators (Shi

210 and Adams 2009).

211   Bromate concentrations were determined by means of ion chromatography with

212 MS/MS detection, using a Shimadzu Prominence LC-20 series HPLC system coupled

213 with an API 4000 QTrap hybrid triple quadrupole/linear ion trap mass spectrometer

214 (AB SCIEX) operating with negative mode electrospray ionization. Separations were

215 performed using an ion exchange column (2×250 mm Dionex IonPac AS-16 w/ $2 \times$

216 50 mm AG-16 guard column) under isocratic conditions, with a mobile phase

217 comprising 20% of a 1 mol/L aqueous methylamine solution and 80% of acetonitrile,

218 at a flow rate of 0.25 mL/min and injection volume of 100 μL. The mass parameters

219 used in multiple reaction monitoring mode for BrO_3^- identification and quantification

220 were $128.9 \rightarrow 113.0$ and $126.9 \rightarrow 110.8$. Method detection and quantification limits for

221 BrO_3^- were 0.03 and 0.1 μg/L, respectively.

222 **3. Results and discussion**

223 **3.1. Degradation of chromophores**

224   Absorbance spectra of water and wastewater ozonated at varying O_3/DOC ratios

225   normalized by the original samples' absorbance spectra are shown in **Figure 1** and

226   **Figure S2**. At all wavelengths > 230 nm, these spectra showed a monotonic decrease

227   of absorbance associated with the increase of ozone dosage. Consistent with previous

228   results (Chon et al. 2015, Gerrity et al. 2012), the normalized absorbance spectra were

229   relatively flat in the wavelength range >250 nm. The flat region in the normalized

230   absorbance spectra could be separated into sub-ranges below ~350 nm and above ~370

231   nm. At low ozone doses (O_3/DOC < 0.4), the observed variations of the normalized

232   absorbance at λ < 350 nm were less pronounced than those of the relative residual

233   absorbance at λ > 370 nm, and such relationships then reversed at the higher O_3/DOC

234   ratios. This phenomenon indicates that the chromophores comprise at least two

235   kinetically distinct functionalities during ozonation (Nanaboina and Korshin 2010).

236   Due to its relatively high absolute value, the UV absorbance in the range of 250-300

237   nm presents a more convenient option for online monitoring than absorbance at λ > 300

238   nm.

239   **Figure 2** illustrates that UVA254 and UVA280 represented as a function of

240   O_3/DOC ratio or ozonation time exhibit similar changes. With the increase of O_3/DOC

241   ratio, the UVA indices decreased steeply at low O_3/DOC ratios (< 0.5 mg O_3/mg DOC)

242   and then decreased more gradually at higher O_3/DOC ratios. When presented vs.

243   ozonation time, the normalized residual UVA indices decreased more steeply at the

244   initial ozonation stage (< 40 s) and more gradually for longer ozonation times. This

245   phenomenon could be explained by the contributions of kinetically different groups of

246 chromophores and also changes of the ozone transfer rate which varied as a function of

247 time (**Figure S1**). The O_3/DOC ratios related to such inflection points were in the range

248 of 0.4-0.6 mg O_3/mg DOC. At these O_3/DOC ratios, UVA254 and UVA280 were

249 decreased by about 45-60 %. Given that the observed changes of the absorbance of

250 ozonated water were similar for the two examined wavelengths, it can be concluded

251 that measurements at 280 nm – a practically implementable LED emission wavelength

252 feasible for online applications – may represent an excellent alternative to UVA254

253 measurements in the context of evaluation of ozonation efficiency as well as DBP

254 formation during chlorination (Li et al. 2016a).

255 **3.2. Degradation of fluorophores**

256   Representative fluorescence excitation-emission matrixes (EEM) of untreated

257 wastewater and surface water samples are shown in **Figure 3**. Generally, the

258 fluorescence peaks with Em<380 nm are ascribed to protein-like fluorescence while the

259 fluorescence peaks with Em>380 nm are ascribed to humic-like fluorescence associated

260 with fluorophores comprising aromatic rings substituted with various electron-donating

261 functional groups (Barsotti et al. 2016, Li et al. 2013, Li et al. 2015).

262   The examined wastewater samples showed the presence of two protein-like

263 fluorescence peaks (Em ~ 350 nm) and two humic-like fluorescence peaks (Em ~ 430

264 nm), while the EEM of Lake Pleasant water was dominated by two humic-like

265 fluorescence peaks (Em ~ 450 nm). The comparison of the fluorescence data obtained

266 with the LED sensor and the lab benchtop spectrometer (**Table S1**) indicates a very

267 good convergence of these results and thus confirms the good sensitivity and accuracy

268 of the LED sensor for use in online monitoring applications. However, the sensitivity

269 of the LED sensor to humic-like fluorescence is much higher than to protein-like

270 fluorescence, mainly due to the fluorescence integration area, the transmittance

271 efficiency of the sensor's bandpass filter, and the response sensitivity of photodiodes to

272 UV light. Due to the relatively weak contribution of protein-like fluorescence in Lake

273 Pleasant samples, measurements of humic-like fluorescence are mainly discussed

274 hereafter.

275   **Figure 4** illustrates the degradation of humic-like fluorophores during ozonation.

276 The humic-like fluorescence decreased very steeply at the initial stage of ozonation

277 time (< 25 s) and then reached to a distinguishable flat region at high ozone time. Like

278 for UVA254 and UVA280, the decrease of humic-like fluorescence as a function of

279 O_3/DOC ratio could also be divided into two stages; however, more than 80% of the

280 humic-like fluorescence was lost in the initial stage – much higher than for the UVA

281 indices. The O_3/DOC ratios related to such inflection points between these two stages

282 were in the range of 0.3-0.4.

283 **3.3. Formation of BDOC**

284   **Figure 5a** presents the formation of $BDOC_{rapid}$ as a function of O_3/DOC ratio or

285 ozonation time. These data demonstrate that the formation of $BDOC_{rapid}$ increased

286 gradually at O_3/DOC ratios < 0.4 and while it increased more steeply for O_3/DOC ratios

287 0.4-0.7. Above the latter transitional range of O_3/DOC ratios, $BDOC_{rapid}$ formation

288 leveled off with distinguishable plateaus at higher O_3/DOC ratios, suggesting that the

15

289 remaining DOM is relatively refractory and requires more O_3 to be converted to the

290 biodegradable form. Similar patterns of BDOC formation at low O_3 doses were

291 observed in prior studies. For instance, Win et al. (2000) found that the biodegradability

292 of DOM was not appreciably affected by ozonation until a threshold of ozone dose was

293 reached. Liu et al. (2015) reported that there was no significant formation of aldehydes

294 and carboxylic acids that comprise a large part of the assimilable organic carbon (AOC)

295 in ozonated wastewater (DOC 7.8 mg/L) with O_3 dose less than 2 mg/L. The plateau in

296 $BDOC_{rapid}$ formation at higher O_3/DOC ratios is also consistent with prior observations

297 (Siddiqui et al. 1997, Treguer et al. 2010). When represented as a function of the

298 decrease of UV absorbance and fluorescence (**Figure 5b&c**), the $BDOC_{rapid}$

299 concentrations increased slowly in the initial stage and then rose more noticeably. The

300 inflection points in these plots corresponding to the decrease of UVA indices and

301 fluorescence were close to 35-45%, and 75-85%, respectively.

302 The degradation of DOM during ozonation can occur through either direct reaction

303 with O_3, or with $^\bullet$OH radical generated during O_3 decomposition (von Gunten 2003a,

304 Wert et al. 2009). During the initial ozone demand stage (**Figure S3**), ozone reacts

305 directly and selectively with electron-rich moieties, e.g., aromatic chromophores or

306 fluorophores (Chon et al. 2015, Wert et al. 2009, Wu et al. 2016), resulting in the rapid

307 decreases of UV absorbance and fluorescence signals (**Figure 2** and **Figure 4**). Prior

308 research based on ozonation experiments (DOC 1.2-1.4 mg/L, O_3 2 mg/L) performed

309 with and without $^\bullet$OH scavengers confirmed that direct ozone reactions are mainly

310 responsible for the formation of small organic compounds contributing to AOC during

311   the initial ozone demand stage (Hammes et al. 2006). However, such AOC molecules

312   might not be produced substantially at very low ozone dose (Liu et al. 2015). In the

313   present work, it is possible that the initial selective attacks of O_3 on electron-rich

314   moieties were not sufficient to break down the large MW DOM fractions into small

315   molecules associated with AOC, leading to the apparent lag in formation of $BDOC_{rapid}$

316   at O_3/DOC ratios < 0.4 The presence of small quantities of inorganic constituents that

317   might exert rapid O_3 demand at low O_3 doses (e.g., NO_2^-) also cannot be ruled out. With

318   greater O_3 doses, increasing exposure to O_3 and $^•OH$ may have led to more extensive

319   breakdown of aromatic structures and other electron-rich targets through direct

320   reactions with O_3 and indirect reactions involving the much less selective $^•OH$ (Legrini

321   et al. 1993, von Gunten 2003a). At O_3/DOC ratios above 0.4-0.7, the observed decrease

322   in formation of $BDOC_{rapid}$ may be attributable to accumulation of more O_3- and $^•OH$-

323   recalcitrant products (e.g., acetic and oxalic acids) (Hammes et al. 2006, Ramseier and

324   Gunten 2009). The synergistic effect of O_3 and $^•OH$ radical contributed to the sufficient

325   decomposition of large MW DOM and the prominent formation of AOCs.

326   **3.4. Evolution of DOM molecular weight during ozonation**

327   **Figure 6** shows the evolution of SEC-OCD chromatograms of WWTP effluent and

328   Lake Pleasant water during ozonation. In SEC experiments, DOM fractions with higher

329   apparent MW have lower elution times (**Figure S4**). Using peak assignments

330   introduced in prior research (Huber et al. 2011) to denote major features observed in

331   the data shown in **Figure 6**, both WWTP effluent and Lake Pleasant water had a

332   biopolymer-like peak of large AMW (peak a1 and peak b1, 20-30 min, AMW > 20

kDa). The WWTP effluent exhibited several peaks in the medium AMW range (peak a2, humic-like peak, 30-36 min, AMW of 14-5.5 kDa; peak a3, peak of building blocks, 36-40 min, AMW of 5.5-3 kDa) and two well-resolved peaks located at lower AMW values (peak a4, peak of low MW acids, 40-48 min, AMW of 3-0.8 kDa; peak a5, peak of low MW neutrals, 50-60 min, AMW < 800 Da). SEC-OCD data for Lake Pleasant water exhibited a prominent peak b2 (humic-like peak, 28-36 min, AMW of 20-5.5 kDa) with a shoulder b3 (building blocks, 36-40 min, AMW of 5.5-3 kDa). These peaks located in the range of medium AMW typically attributed to humic substances were responsible for a large portion of DOC in untreated Lake Pleasant water. The SEC-OCD of Lake Pleasant water also had two weaker peaks located in the range of small AMW (peak b4 and peak b5), which are designated as low MW acids and neutrals.

The evolution of apparent DOM molecular weights is indicated by the red arrows in **Figure 6.** It is also visualized using 2D synchronous correlation contours (**Figure S5**). At increasing ozone dosages, the large MW biopolymer-like peaks (a1 and b1) and medium MW humic-like peaks (a2 and b2) decreased while the concentration of building blocks and low MW acids and neutrals increased, suggesting that the larger AMW DOM components were transformed into smaller AMW species during ozonation. The newly formed medium building blocks and small MW DOM species were easily biodegraded and mainly contributed to the $BDOC_{rapid}$ (**Figure S6**). The SEC-OCD results also confirmed that the decomposition of biopolymer-like or humic-like peaks was not prominent (<20%) during the initial ozonation stage, despite the substantial losses of UVA and fluorescence (**Figure S7**).

3.5. Formation of bromate

Figures 7a-b depict bromate yields (expressed as mol ratios of Br associated with BrO_3^- to initial Br^- ($[BrO_3^-]/[Br^-]$, in % mol/mol) plotted as a function of O_3/DOC ratio or ozonation time. The observed relationships exhibit the presence of two phases of bromate formation, as marked by the dash line. During the initial phase (O_3/DOC ratios < 0.4 or ozonation time < 25 s), bromate yields were low ($[BrO_3^-]/[Br^-]$ < 2 %) and effects of initial Br^- concentrations on this phase were minor. This is in agreement with the data of previous studies (Chon et al. 2015, Soltermann et al. 2016), which observed a negligible bromate yield (≤3%) for O_3/DOC ratios < 0.4-0.6 mg O_3/mg DOC.

This phenomenon can be ascribed to specific features of the formation pathway of bromate, which is generated via a complex mechanism involving ozone and hydroxyl radical (Fischbacher et al. 2015, von Gunten and Oliveras 1998). During the initial phase of bromate formation (O_3/DOC ratios < 0.4, ozonation time < 25 s), O_3 is rapidly consumed by electron-rich moieties (Buffle et al. 2006, Lee et al. 2013) whose consumption is consistent with the rapid decrease of humic-like fluorescence (**Figure 4**), thus leaving little residual O_3 for reaction with Br^- (**Figure S3**). In the second phase, in which measured residual ozone concentrations exceeded 1 mg/L (**Figure S3**), bromide could be readily oxidized to bromate, with its yields increasing with the ozone doses, and different water matrixes had a significant effect on the bromate yields measured as a function of O_3/DOC ratio or ozonation time.

When plotted versus O_3/DOC ratio, the bromate formation across different water

376   matrixes was similar for each matrix when presented in terms of bromate concentration

377   in µg/L (**Figure S8**), but different when represented in terms of bromate yield units

378   (**Figure 7**). That is, the lower initial bromide concentration in Lake Pleasant water led

379   to higher molar bromate yields compared to those for the higher-bromide WWTP

380   effluent samples at the same ozone doses. Compared with the data of the previous study

381   (Chon et al. 2015), the bromate formation yields of WWTP effluent samples at the

382   corresponding O_3/DOC ratios in the present work were lower, possibly due to the higher

383   initial Br^- concentrations in this study (Br^- 300-500 µg/L for DOC 5.8-6.9 mg/L vs. Br^-

384   39-86 µg/L for DOC 5.3-7.3 mg/L). Therefore, the O_3/DOC ratio might not always be

385   an optimal indicator for estimation of bromate formation across different water matrixes.

386   **Figures 7c-d** present the normalized bromate yields ($[BrO_3^-]/[Br^-]$, mol/mol) as a

387   function of relative changes in the spectroscopic parameters UVA254, UVA280 and

388   humic-like fluorescence. In agreement with one previous study (Chon et al. 2015), the

389   plots of bromate yields vs. spectroscopic indicators overlapped for all data sets obtained

390   in the ozonation experiments, although the DOM properties and initial Br^-

391   concentrations were different. Similarly to the observations discussed above, changes

392   in the bromate yields could be further divided into two stages characterized by

393   significantly different slopes vs. corresponding spectroscopic index. The inflection

394   points related to the appreciable formation of BrO_3^- were in the range of 45-55%, 50-

395   60% and 86-92% losses of UVA254, UVA280, and humic-like fluorescence,

396   respectively. Unlike O_3/DOC ratios, the plots of $[BrO_3^-]/[Br^-]$ as a function of the

397   spectroscopic indicators in the second phase had relatively small differences for the

398 data obtained for Lake Pleasant and WWTP effluent samples, suggesting that the

399 spectroscopic indices may be more suitable as a surrogate parameter for bromate

400 formation in waters of varying composition.

401   With respect to the US EPA's MCL for BrO_3^- in drinking water of 10 μg/L, the

402 breakthrough points related to removals of UVA254, UVA280 and decrease of humic-

403 like fluorescence were in the range of 45-55%, 52-57%, and 86-90%, respectively

404 (**Figure 8**). In contrast to the observations made for $[BrO_3^-]/[Br^-]$ molar yields (**Figure**

405 **7**), plots of BrO_3^- vs UVA254 and BrO_3^- vs UVA280 diverged into distinct groups of

406 data for WWTP effluents and Lake Pleasant. Such divergences were presumably due

407 to differences in initial Br^- concentrations in the various matrixes, since BrO_3^- yields

408 were not normalized to initial Br^- levels in these plots. Additionally, chromophores in

409 Lake Pleasant water appeared to be much more susceptible to the oxidation at higher

410 O_3 exposures than chromophores in WWTP effluents (**Figure 2**). However, no

411 significant divergences between the data for dissimilar water matrixes were observed

412 in plots of BrO_3^- vs humic fluorescence. In comparison to the ~25% variation amongst

413 UVA indices in the various matrixes at higher O_3 exposures, further decreases of

414 humic-like fluorescence were limited in a narrow range from 90% to 100%. The

415 association of this narrow range of changes of humic-like fluorescence with the

416 generation of bromate is likely to have largely eliminated any divergence attributable

417 to differences in initial Br^- concentration. A previous study also reported a sole

418 correlation between a fluorescence index and several chlorinated DBPs regardless of

419 the water source and treatment, while the differential absorbance correlations could be

420 interfered by many species (Roccaro et al. 2009). These results showed that

421 fluorescence indices may have more advantages than absorbance indices in actual water

422 systems.

423   The plots of BrO_3^- concentration (μg/L) versus decrease of humic fluorescence (HS,

424 in %) were fitted by MATLAB software (**Figure S9**), and an empirical equation

425 applicable to the ranges of 6-7 mg/L DOC and 100-500 μg/L Br^- was obtained, as

426 presented below:

427      $$BrO_3^- \ (\text{μg/L}) = 7.64 * 10^{-9} * e^{0.237*HS(\%)} \ , R^2 = 0.962$$

428   The results of this study suggest that measurements of changes in humic-like

429 fluorescence of ozonated water are highly suitable for the estimation of bromate

430 formation in dissimilar water matrixes. The results in **Figure S10** further indicate that

431 DOC concentration has relatively little effect on the relationships between bromate

432 formation and humic-like fluorescence. However, the robustness of such relationships

433 still needs to be explored in the future; for example, with respect to the effects of pH,

434 temperature, DOC and NH_4^+ concentrations.

435   In the context of optimization of ozone dosage, the typical goal is to maximize the

436 effect of oxidation while simultaneously minimizing the formation of undesired

437 byproducts. Gerrity et al. (2012) previously reported that ~50% reduction of UVA254

438 or ~90% decrease of total fluorescence were required to reach acceptable levels of

439 pathogen inactivation and sufficient elimination of many micropollutants. The present

440 work supports these findings and demonstrates possible approaches for assessing the

441   potential formation of BDOC and bromate during water and wastewater ozonation,

442   especially for water having bromide concentrations above 50 μg/L.

443   **4. Conclusions**

444   ● When represented as a function of changes of spectroscopic indicators such as

445   UVA254, UVA280, and humic-like fluorescence, BDOC concentrations initially

446   increased slowly and then rose more noticeably. The inflection points indicative of

447   BDOC formation threshold were located in the range of 35-45% loss of UVA254

448   or UVA280 and 75-85% loss of humic-like fluorescence.

449   ● SEC-OCD data showed that large biopolymer molecules in WWTP effluent

450   (apparent MW>20 kDa) and medium-AMW humic substances in Lake Pleasant

451   surface water (AMW 5.5-20 kDa) were transformed into medium-AMW building

452   blocks and small AMW species associated with BDOC.

453   ● When represented as a function of spectroscopic indicators, the inflection points

454   that corresponded to the onset of bromate formation were approximately 45-55%,

455   50-60% and 86-92% for decreases in UVA254, UVA280 and humic fluorescence,

456   respectively.

457   ● An empirical equation modeling the relationship between bromate concentrations

458   (expressed in μg/L) and concomitant decreases of humic-like fluorescence (%) was

459   established based on the data generated for wastewater effluent and surface water

460   that had 100 to 500 μg/L Br⁻.

461   ● The results suggest that measurements of UVA280 and humic-like fluorescence

462   complement conventional UVA254 measurements, especially in the context of

463   assessing the formation of BDOC and bromate. The use of these spectroscopic

464   parameters is expected to be enhanced by the recent development of

465   online/portable spectrometers that use LEDs as a light source.

466   **Acknowledgement**

474   **Appendix A. Supplementary data**

475   Supplementary data related to this article can be found in Supporting Information.

476 **References**

477 Bader, H. and Hoigné, J., 1981. Determination of ozone in water by the indigo method.

478   Water Research 15 (4), 449-456.

479 Barsotti, F., Ghigo, G. and Vione, D., 2016. Computational assessment of the

480   fluorescence emission of phenol oligomers: A possible insight into the

481   fluorescence properties of humic-like substances (HULIS). Journal of

482   Photochemistry and Photobiology a-Chemistry 315, 87-93.

483 Black, K.E. and Berube, P.R., 2014. Rate and extent NOM removal during oxidation

484   and biofiltration. Water Research 52, 40-50.

485 Bridgeman, J., Baker, A., Brown, D. and Boxall, J.B., 2015. Portable LED fluorescence

486   instrumentation for the rapid assessment of potable water quality. Science of The

487   Total Environment 524–525, 338-346.

488 Buffle, M.-O., Schumacher, J., Salhi, E., Jekel, M. and von Gunten, U., 2006.

489   Measurement of the initial phase of ozone decomposition in water and wastewater

490   by means of a continuous quench-flow system: Application to disinfection and

491   pharmaceutical oxidation. Water Research 40 (9), 1884-1894.

492 Butler, R., Godley, A., Lytton, L. and Cartmell, E., 2005. Bromate environmental

493   contamination: Review of impact and possible treatment. Critical Reviews in

494   Environmental Science and Technology 35 (3), 193-217.

495 Chin, Y.-P., Aiken, G. and O'Loughlin, E., 1994. Molecular Weight, Polydispersity,

496   and Spectroscopic Properties of Aquatic Humic Substances. Environmental

497   Science & Technology 28 (11), 1853-1858.

498   Chiou, C.F., Marinas, B.J. and Adams, J.Q., 1995. Modified indigo method for gaseous

499   and aqueous ozone analyses. Ozone-Science & Engineering 17 (3), 329-344.

500   Chon, K., Salhi, E. and von Gunten, U., 2015. Combination of UV absorbance and

501   electron donating capacity to assess degradation of micropollutants and formation

502   of bromate during ozonation of wastewater effluents. Water Research 81, 388-397.

503   Dodd, M.C., Kohler, H.P.E. and von Gunten, U., 2009. Oxidation of Antibacterial

504   Compounds by Ozone and Hydroxyl Radical: Elimination of Biological Activity

505   during Aqueous Ozonation Processes. Environmental Science & Technology 43

506   (7), 2498-2504.

507   Escobar, I.C. and Randall, A.A., 2001. Assimilable organic carbon (AOC) and

508   biodegradable dissolved organic carbon (BDOC): Complementary measurements.

509   Water Research 35 (18), 4444-4454.

510   Fimmen, R.L., Cory, R.M., Chin, Y.-P., Trouts, T.D. and McKnight, D.M., 2007.

511   Probing the oxidation–reduction properties of terrestrially and microbially derived

512   dissolved organic matter. Geochimica et Cosmochimica Acta 71 (12), 3003-3015.

513   Fischbacher, A., Loeppenberg, K., von Sonntag, C. and Schmidt, T.C., 2015. A New

514   Reaction Pathway for Bromite to Bromate in the Ozonation of Bromide.

515   Environmental Science & Technology 49 (19), 11714-11720.

516   Gerrity, D., Gamage, S., Jones, D., Korshin, G.V., Lee, Y., Pisarenko, A., Trenholm,

517   R.A., von Gunten, U., Wert, E.C. and Snyder, S.A., 2012. Development of

518   surrogate correlation models to predict trace organic contaminant oxidation and

519   microbial inactivation during ozonation. Water Research 46 (19), 6257-6272.

520 Hammes, F., Salhi, E., Koster, O., Kaiser, H.P., Egli, T. and von Gunten, U., 2006.

521 Mechanistic and kinetic evaluation of organic disinfection by-product and

522 assimilable organic carbon (AOC) formation during the ozonation of drinking

523 water. Water Research 40 (12), 2275-2286.

524 Henderson, R.K., Baker, A., Murphy, K.R., Hambly, A., Stuetz, R.M. and Khan, S.J.,

525 2009. Fluorescence as a potential monitoring tool for recycled water systems: A

526 review. Water Research 43 (4), 863-881.

527 Hollender, J., Zimmermann, S.G., Koepke, S., Krauss, M., McArdell, C.S., Ort, C.,

528 Singer, H., von Gunten, U. and Siegrist, H., 2009. Elimination of Organic

529 Micropollutants in a Municipal Wastewater Treatment Plant Upgraded with a Full-

530 Scale Post-Ozonation Followed by Sand Filtration. Environmental Science &

531 Technology 43 (20), 7862-7869.

532 Huber, M.M., Gobel, A., Joss, A., Hermann, N., Loffler, D., McArdell, C.S., Ried, A.,

533 Siegrist, H., Ternes, T.A. and von Gunten, U., 2005. Oxidation of pharmaceuticals

534 during ozonation of municipal wastewater effluents: A pilot study. Environmental

535 Science & Technology 39 (11), 4290-4299.

536 Huber, S.A., Balz, A., Abert, M. and Pronk, W., 2011. Characterisation of aquatic

537 humic and non-humic matter with size-exclusion chromatography – organic

538 carbon detection – organic nitrogen detection (LC-OCD-OND). Water Research

539 45 (2), 879-885.

540 Lee, C.O., Howe, K.J. and Thomson, B.M., 2012. Ozone and biofiltration as an

541 alternative to reverse osmosis for removing PPCPs and micropollutants from

542   treated wastewater. Water Research 46 (4), 1005-1014.

543   Lee, Y., Gerrity, D., Lee, M., Bogeat, A.E., Salhi, E., Gamage, S., Trenholm, R.A.,

544   Wert, E.C., Snyder, S.A. and von Gunten, U., 2013. Prediction of Micropollutant

545   Elimination during Ozonation of Municipal Wastewater Effluents: Use of Kinetic

546   and Water Specific Information. Environmental Science & Technology 47 (11),

547   5872-5881.

548   Legrini, O., Oliveros, E. and Braun, A.M., 1993. Photochemical processes for water

549   treatment. Chemical Reviews 93 (2), 671-698.

550   Li, W.-T., Jin, J., Li, Q., Wu, C.-F., Lu, H., Zhou, Q. and Li, A.-M., 2016a. Developing

551   LED UV fluorescence sensors for online monitoring DOM and predicting DBPs

552   formation potential during water treatment. Water Research 93, 1-9.

553   Li, W.-T., Xu, Z.-X., Li, A.-M., Wu, W., Zhou, Q. and Wang, J.-N., 2013.

554   HPLC/HPSEC-FLD with multi-excitation/emission scan for EEM interpretation

555   and dissolved organic matter analysis. Water Research 47 (3), 1246-1256.

556   Li, W., Nanaboina, V., Chen, F. and Korshin, G.V., 2016b. Removal of polycyclic

557   synthetic musks and antineoplastic drugs in ozonated wastewater: Quantitation

558   based on the data of differential spectroscopy. Journal of Hazardous Materials 304,

559   242-250.

560   Li, W., Xu, Z., Wu, Q., Li, Y., Shuang, C. and Li, A., 2015. Characterization of

561   fluorescent-dissolved organic matter and identification of specific fluorophores in

562   textile effluents. Environmental Science and Pollution Research 22 (6), 4183-4189.

563   Liu, C., Nanaboina, V. and Korshin, G., 2012a. Spectroscopic study of the degradation

564   of antibiotics and the generation of representative EfOM oxidation products in

565   ozonated wastewater. Chemosphere 86 (8), 774-782.

566   Liu, C., Nanaboina, V., Korshin, G.V. and Jiang, W., 2012b. Spectroscopic study of

567   degradation products of ciprofloxacin, norfloxacin and lomefloxacin formed in

568   ozonated wastewater. Water Research 46 (16), 5235-5246.

569   Liu, C., Tang, X., Kim, J. and Korshin, G.V., 2015. Formation of aldehydes and

570   carboxylic acids in ozonated surface water and wastewater: A clear relationship

571   with fluorescence changes. Chemosphere 125, 182-190.

572   Nakada, N., Shinohara, H., Murata, A., Kiri, K., Managaki, S., Sato, N. and Takada, H.,

573   2007. Removal of selected pharmaceuticals and personal care products (PPCPs)

574   and endocrine-disrupting chemicals (EDCs) during sand filtration and ozonation

575   at a municipal sewage treatment plant. Water Research 41 (19), 4373-4382.

576   Nanaboina, V. and Korshin, G.V., 2010. Evolution of Absorbance Spectra of Ozonated

577   Wastewater and Its Relationship with the Degradation of Trace-Level Organic

578   Species. Environmental Science & Technology 44 (16), 6130-6137.

579   Nie, Y., Hu, C., Li, N., Yang, L. and Qu, J., 2014. Inhibition of bromate formation by

580   surface reduction in catalytic ozonation of organic pollutants over beta-

581   FeOOH/Al2O3. Applied Catalysis B-Environmental 147, 287-292.

582   Nishijima, W., Fahmi, Mukaidani, T. and Okada, M., 2003. DOC removal by multi-

583   stage ozonation-biological treatment. Water Research 37 (1), 150-154.

584   Noda, I. and Ozaki, Y. (2005) Two-dimensional correlation spectroscopy: applications

585   in vibrational and optical spectroscopy, John Wiley & Sons.

586   Peter, A. and von Gunten, U., 2007. Oxidation kinetics of selected taste and odor

587   compounds during ozonation of drinking water. Environmental Science &

588   Technology 41 (2), 626-631.

589   Ramseier, M.K. and Gunten, U.v., 2009. Mechanisms of Phenol Ozonation—Kinetics

590   of Formation of Primary and Secondary Reaction Products. Ozone: Science &

591   Engineering 31 (3), 201-215.

592   Reungoat, J., Escher, B.I., Macova, M., Argaud, F.X., Gernjak, W. and Keller, J., 2012.

593   Ozonation and biological activated carbon filtration of wastewater treatment plant

594   effluents. Water Research 46 (3), 863-872.

595   Roccaro, P., Vagliasindi, F.G.A. and Korshin, G.V., 2009. Changes in NOM

596   Fluorescence Caused by Chlorination and their Associations with Disinfection by-

597   Products Formation. Environmental Science & Technology 43 (3), 724-729.

598   Shi, H. and Adams, C., 2009. Rapid IC–ICP/MS method for simultaneous analysis of

599   iodoacetic acids, bromoacetic acids, bromate, and other related halogenated

600   compounds in water. Talanta 79 (2), 523-527.

601   Siddiqui, M.S., Amy, G.L. and Murphy, B.D., 1997. Ozone enhanced removal of

602   natural organic matter from drinking water sources. Water Research 31 (12), 3098-

603   3106.

604   Soltermann, F., Abegglen, C., Götz, C. and von Gunten, U., 2016. Bromide Sources

605   and Loads in Swiss Surface Waters and Their Relevance for Bromate Formation

606   during Wastewater Ozonation. Environmental Science & Technology 50 (18),

607   9825-9834.

608   Tedetti, M., Joffre, P. and Goutx, M., 2013. Development of a field-portable

609   fluorometer based on deep ultraviolet LEDs for the detection of phenanthrene- and

610   tryptophan-like compounds in natural waters. Sensors and Actuators B-Chemical

611   182, 416-423.

612   Treguer, R., Tatin, R., Couvert, A., Wolbert, D. and Tazi-Pain, A., 2010. Ozonation

613   effect on natural organic matter adsorption and biodegradation - Application to a

614   membrane bioreactor containing activated carbon for drinking water production.

615   Water Research 44 (3), 781-788.

616   von Gunten, U., 2003a. Ozonation of drinking water: Part I. Oxidation kinetics and

617   product formation. Water Research 37 (7), 1443-1467.

618   von Gunten, U., 2003b. Ozonation of drinking water: Part II. Disinfection and by-

619   product formation in presence of bromide, iodide or chlorine. Water Research 37

620   (7), 1469-1487.

621   von Gunten, U. and Oliveras, Y., 1998. Advanced Oxidation of Bromide-Containing

622   Waters: Bromate Formation Mechanisms. Environmental Science & Technology

623   32 (1), 63-70.

624   Wert, E.C., Rosario-Ortiz, F.L., Drury, D.D. and Snyder, S.A., 2007. Formation of

625   oxidation byproducts from ozonation of wastewater. Water Research 41 (7), 1481-

626   1490.

627   Wert, E.C., Rosario-Ortiz, F.L. and Snyder, S.A., 2009. Using Ultraviolet Absorbance

628   and Color To Assess Pharmaceutical Oxidation during Ozonation of Wastewater.

629   Environmental Science & Technology 43 (13), 4858-4863.

630 Wu, Q., Li, W.T., Yu, W.H., Li, Y. and Li, A.M., 2016. Removal of fluorescent

631   dissolved organic matter in biologically treated textile wastewater by ozonation-

632   biological aerated filter. Journal of the Taiwan Institute of Chemical Engineers 59,

633   359-364.

634 Zimmermann, S.G., Wittenwiler, M., Hollender, J., Krauss, M., Ort, C., Siegrist, H. and

635   von Gunten, U., 2011. Kinetic assessment and modeling of an ozonation step for

636   full-scale municipal wastewater treatment: Micropollutant oxidation, by-product

637   formation and disinfection. Water Research 45 (2), 605-617.

638

639 **Table 1. Basic characteristics of water matrixes**

Parameters	WWTP-I	WWTP-II	Lake Pleasant
pH	6.92	6.95	7.48 [a]
DOC (mg/L)	5.82	6.93	14.87
UV254 (cm^{-1})	0.130	0.139	0.727
UV280 (cm^{-1})	0.100	0.108	0.545
Conductivity (us/cm)	480	652	314
Br$^-$ (µg/L) [b]	267.8	201.5	36.7

[a] The pH values of 2.5 times diluted lake Pleasant water were about 7.

[b] The values listed here are the native background Br$^-$ concentrations for each water matrix. Initial Br$^-$ concentrations during ozonation batch experiments, using samples of each water matrix fortified with additional bromide, were as follows: 322.9 µg/L for WWTP-A, 373.8 µg/L for WWTP-B, 491.6 µg/L for WWTP-C, 301.5 µg/L for WWTP-D, and 116.1 µg/L for LP.

640

Figure Captions

Figure 1. Changes in the absorbance spectra of WWTP effluent as a function of O_3/DOC ratio normalized by the absorbance prior to treatment

Figure 2. Decreases of the normalized residual UVA indices as a function of O_3/DOC ratio (or ozonation time – inserts): (a) UVA254 and (b) UVA280

Figure 3. EEM spectra of (a) WWTP-I, (b) WWTP-II, and (c) LP. The circles on the left of each graph represent protein-like fluorescence that the LED sensor measures, while the circles on the right of each graph represent humic-like fluorescence that the LED sensor measures.

Figure 4. Decrease of the normalized humic-like fluorescence (H/H_0) as a function of O_3/DOC ratio or ozonation time (insert) in different ozonation experiments

Figure 5. Formation of $BDOC_{rapid}$ as a function of (a) O_3/DOC ratio or ozonation time (insert), (b) decrease of UVA254 or UVA280 (insert) and (c) decrease of LED humic-like fluorescence

Figure 6. Evolution of SEC-OCD chromatograms of the ozonated wastewater and surface water as a function of O_3/DOC ratio：(a) WWTP-I effluent (WWTP-A) and (b) Lake Pleasant water (LP).

Figure 7. Bromate formation yields ($[BrO_3^-]/[Br^-]$, mol/mol in %) represented as a function of (a) O_3/DOC ratio, (b) ozonation time, (c) decrease of UVA254 or UVA280 (insert) and (d) decrease of LED humic-like fluorescence.

Figure 8. Bromate formation (μg/L) as a function of decreases of spectral indicators: (a) UVA254 or UVA280 (insert) and (b) LED humic-like fluorescence
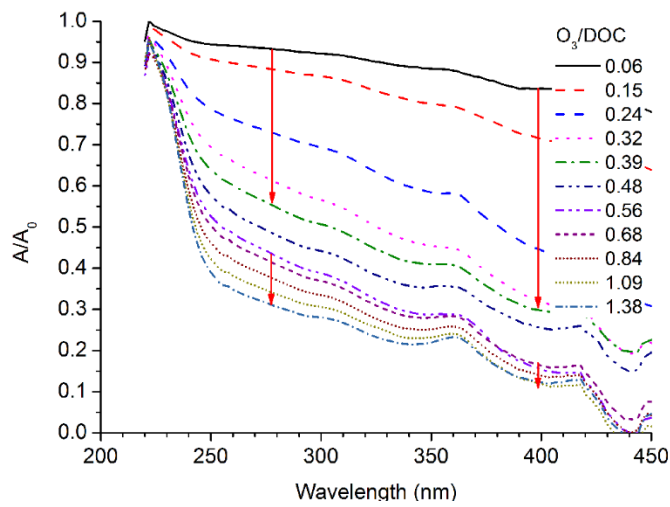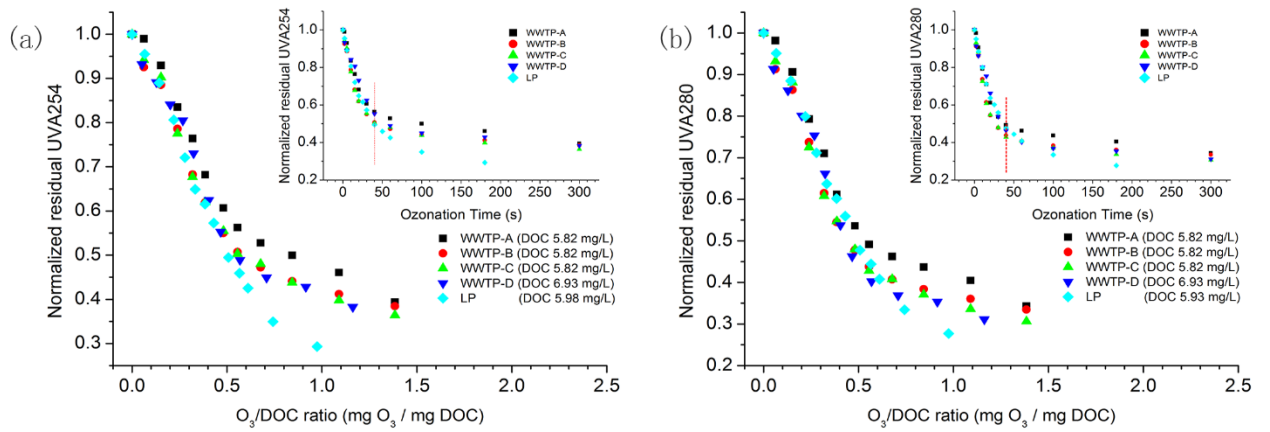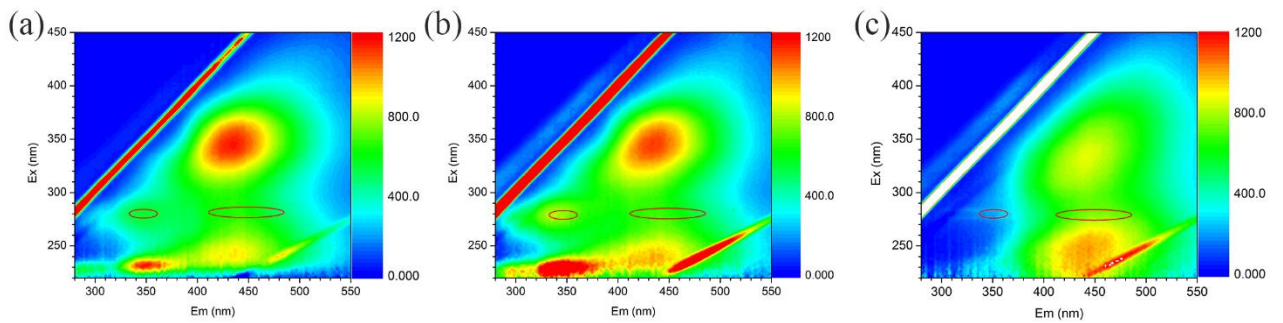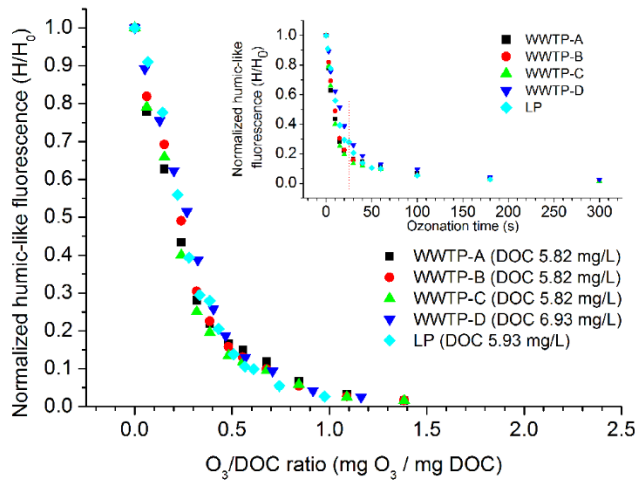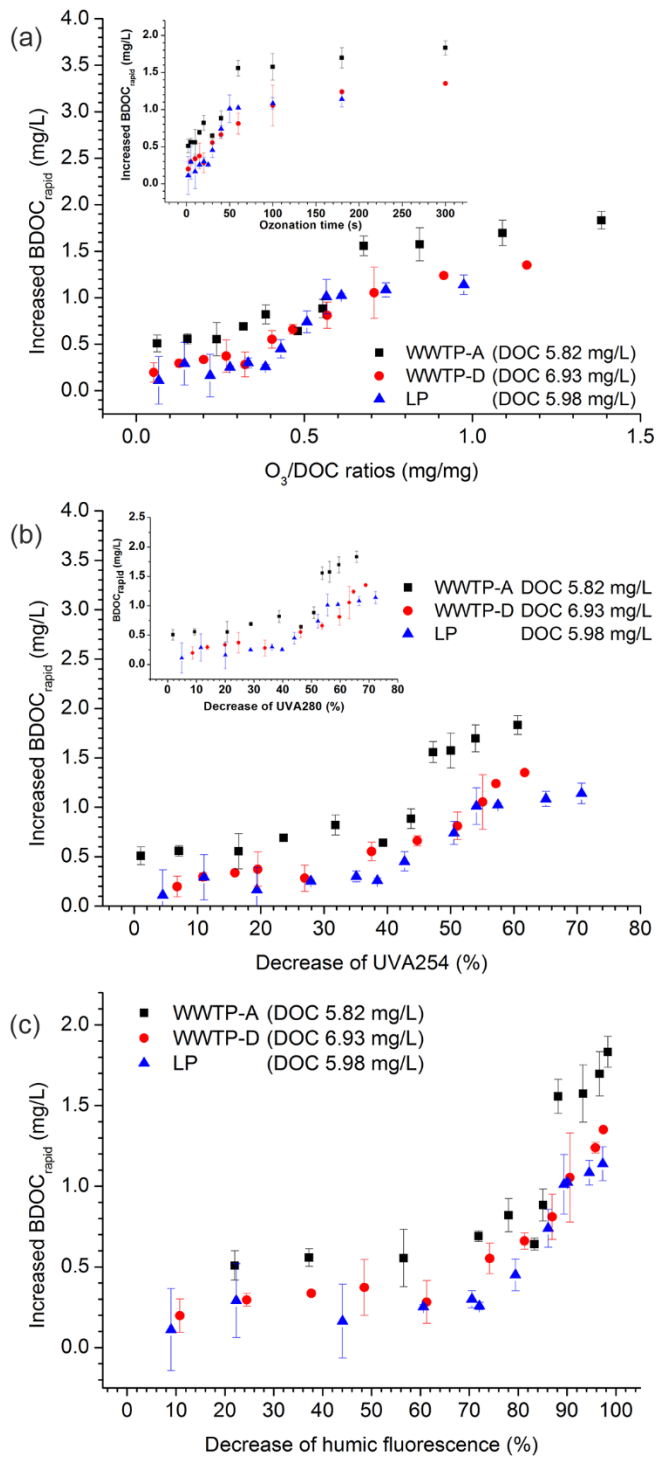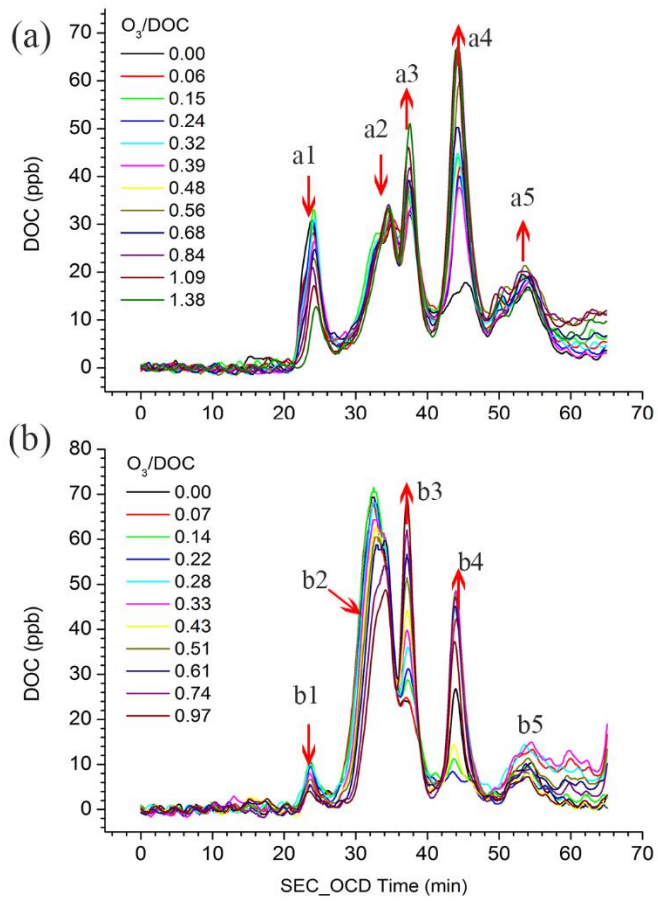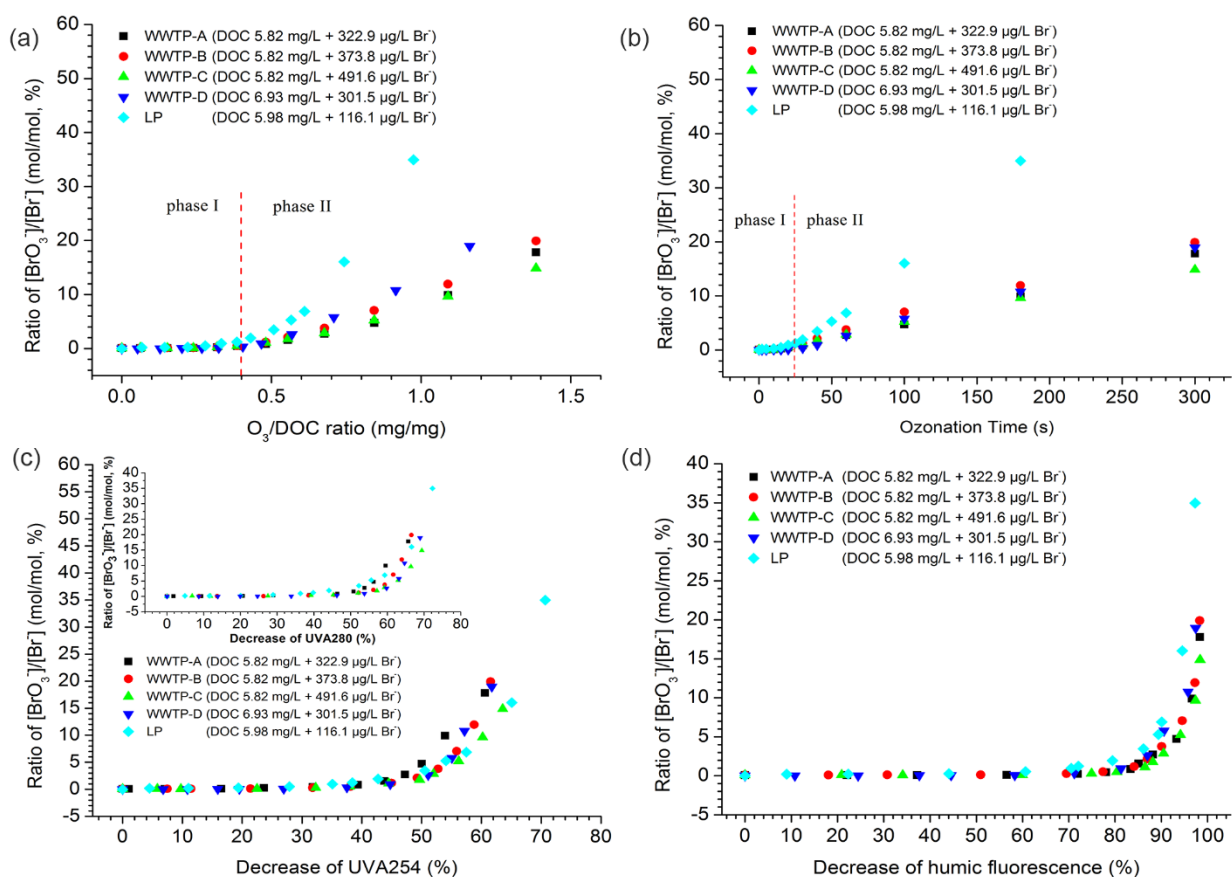
Figure 1

Figure 2

Figure 3

Figure 4

Figure 5

Figure 6

Figure 7

Figure 8